Analysis of Multidimensional Models of Monolith Catalysts for Hybrid Combustors

G. Groppi, A. Belloli, E. Tronconi, and P. Forzatti
Dipartimento di Ingegneria Chimica e Chimica Industriale "G. Natta," Politecnico di Milano, 20133 Milano, Italy

Distributed parameter models of the single channel of a monolith combustor have been derived from progressively simplified assumptions. Simulation results are compared to assess the importance of the different physicochemical phenomena occurring in the combustor and to identify the simplest adequate model. For typical operating conditions of the hybrid combustor (gas and wall temperature not exceeding 1,073 and 1,273 K, respectively, high flow rate and pressure, natural gas as fuel), the results show that variations of gas properties have to be considered while homogeneous combustion can be neglected. Assumption of the approximate radial profile of axial velocity with invariant parabolic shape, rather than the rigorous solution of momentum balance and the continuity equation, provides accurate results. Moreover, for simulation of ceramic monoliths, backward heat transmission by wall conduction can be neglected with a substantial saving of computational labor.

Introduction

Catalytic combustion is currently considered a promising method for the simultaneous reduction of NO_x, CO, and unburnt hydrocarbons (UHC) emissions from gas turbines.

The process is based on the catalyst capability to lower the ignition temperature of fuel–air mixtures and to operate with low fuel concentrations (Trimm, 1983; Prasad et al., 1984; Pfefferle and Pfefferle, 1987). This process has been realized and tested at an early stage with different combustor configurations. In the so-called catalytically stabilized thermal (CST) combustor (Pfefferle and Pfefferle, 1987) a premixed and preheated fuel–air stream passes through a catalyst bed where combustion proceeds till complete fuel consumption, first via heterogeneous reaction, and then downstream in the bed, where temperatures are high enough to ignite gas-phase combustion, via simultaneous catalytic and homogeneous reaction. Despite the ultralow emissions achieved in preliminary tests (< 2 ppm of NO_x with a few ppm of CO and UHC), this configuration appears too demanding from the standpoint of midterm industrial development: the catalyst should guarantee stable performances for long-time operation at 1,573 K and in the presence of severe thermal shocks. The hybrid combustor (Furuya et al., 1987; Ozawa et al., 1991) aims at the reduction of the thermal stresses of the catalytic materials. In this configuration the catalytic and the homogeneous reactions are carried out in two distinct sections. Only a fraction of the fuel is fed to the catalyst after being premixed with preheated air, while the remaining fraction is fed, by premixing nozzles, to a downstream homogeneous section. The fuel-to-air ratio in the catalyst feed is constrained to prevent the catalyst temperature (the adiabatic reaction temperature) to exceed 1,273 K, thus softening catalyst thermal stresses. The hot gas stream exiting the catalyst enhances the stability of the gas-phase combustion in the downstream section so that high combustion efficiencies can be attained at lower temperatures than those allowable in current gas turbine combustors, resulting in very low NO_x emissions.

In all the combustor configurations the catalytic reaction is carried out in monoliths in order to meet the gas turbine requirements on pressure drop. In principle the following phenomena occur in the monolith channels: (1) heterogeneous reactions at the catalyst wall and homogeneous reactions in the gas phase; (2) heat, mass, and momentum transfer by convection and diffusion in the gas phase and at the gas–solid interface; (3) mass diffusion in catalyst pores; (4) heat transfer by conduction and radiation in the solid. Strong interactions occur between these phenomena due to the intense thermal effects associated with the heat of combustion.

Multidimensional models have been described and solved (Young and Finlayson, 1976; Heck et al., 1976; Lee and Aris, 1977; Bruno et al., 1983; Hayes et al., 1992). In some of these articles (Young and Finlayson, 1976; Heck et al. 1976; Lee and Aris, 1977) constant physicochemical properties of the

Correspondence concerning this article should be addressed to P. Forzatti.

gas are assumed in spite of significant temperature variations. These works refer to the analysis of catalytic mufflers where T-gradients are less severe than in catalytic combustors for gas turbines. The effect of wall conduction was studied by Young and Finlayson (1976) and by Lee and Aris (1977), who also addressed the effect of radiation, showing that radiative heat transfer can be accounted for by properly increasing the wall heat conduction. However the results reported therein cannot be directly extended to the simulation of catalytic combustors for gas turbines because of the markedly different operating conditions, which affect the relative importance of heat transport mechanisms.

The effect of property variation on the behavior of the monolithic catalyst has not been completely assessed yet. Hayes and coworkers (Hayes et al., 1992) have considered the temperature dependence of gas density, heat capacity, mass, and thermal diffusivity, but they have neglected the effect of viscosity variation on the shape of the velocity profiles. They refer to leaner fuel–air mixtures than those typical of gas turbine combustion, and in any case they do not report any comment on the effects of property variations. Bruno and coworkers (Bruno et al., 1983) have developed a model of a monolith combustor for power applications that includes momentum balance equations and rigorously accounts for the variations of the gas properties with temperature. However, they have assumed an infinitely fast reaction at the catalytic wall; thus their model does not provide any indication of the effect of gas property variations on the location of the catalytic light-off. Anyway they report that model predictions are sensitive to the exponent of the power law dependence of mass diffusivity on temperature, which indicates that property variations significantly affect the simulation results.

The computational labor for the solution of the governing equations of rigorous models is sufficiently heavy to make any reasonable approximation attractive. This work addresses the importance of different physicochemical phenomena for modeling the catalyst section of a hybrid combustor, aiming at the identification of the simplest adequate mode. The results of rigorous and simplified multidimensional models have been compared for this purpose. The effects of hydrodynamical development, gas property variations, wall heat conduction, and radiation (and homogeneous reaction) have been investigated. Simulations have been performed for parameter values corresponding to typical operating conditions and geometry of the channels of the monolith combustor (Table 1). Assumed gas velocities correspond to the lower values of the typical operating range (10 m/s), so as to remain in laminar flow conditions.

Table 1. Typical Operating Conditions and Geometric Parameters for the Catalytic Section of Hybrid Combustors

T gas inlet at the catalytic section	623–773 K
T gas outlet at the catalytic section	1,073 K
Maximum catalyst temperature	1,273 K
% fuel (CH_4) molar fraction at catalyst inlet	1.8–2.3
Pressure	10–15 atm
Inlet gas velocity*	7–40 m/s
Open frontal area (ϵ)	0.65–0.68
Diameter of the channel	1–3 mm
Channel length	7.5–12 cm

*Referred to the cross section immediately upstream the catalyst inlet.

Model Development

Assumptions

The monolith is composed of a large number of parallel channels whose conditions are supposed to be identical when assuming global adiabaticity and uniform distribution of variables at the monolith inlet. Under these hypotheses the simulation of the whole monolith reduces to the analysis of a single channel. Accordingly multidimensional models of the single monolith channel have been developed.

For the study of the effects of the hydrodynamical development and of the gas property variations, four different two-dimensional (2-D) models for channels with circular cross section have been developed. The most detailed one, referred to in the following as IId, considers the temperature dependence of the gas properties and includes momentum balance and continuity equations in addition to mass and enthalpy balances. The boundary layer approximation (Schlichting, 1955) has been adopted, Peclet numbers in the monolith channels of a hybrid combustor being typically > 1,000. According to the *a posteriori* analysis performed by Worsøe-Schmidt and Leppert (1965), for such Peclet numbers the boundary layer approximation is correct after a heated length of 0.5 diameters. Buoyancy forces have been neglected in the momentum balance, being $Gr/Re < 3$ (Worsøe-Schmidt and Leppert, 1965). The equations of state of ideal gases have been used and the temperature dependence of the gas properties has been approximated with power laws (the T-dependence of heat capacity has been neglected):

$$\frac{k_{t_g}}{k_{t_g}^0} = \left(\frac{T}{T^0}\right)^{0.75} \qquad \frac{D_f}{D_f^0} = \left(\frac{T}{T^0}\right)^{1.75} \qquad \frac{\mu_f}{\mu_f^0} = \left(\frac{T}{T^0}\right)^{0.67}. \quad (1)$$

The simplest 2-D model (IIa) has been developed under the assumptions of fully developed laminar flow and constant gas properties.

Intermediate models IIb and IIc consider the temperature dependence of gas density (ideal gas), mass diffusivity, and thermal conductivity. Due to the temperature rise, gas density decreases along the axial coordinate, so that the axial velocity has to increase to satisfy the global mass balance on the cross sections. In order to significantly reduce the computational effort, Models IIb and IIc do not include momentum balance and continuity equations, and the variations of the axial velocity profiles are calculated under the following hypotheses.

Model IIb. The specific mass-flow rate in each radial annulus is maintained constant throughout the reactor. Assuming a parabolic, fully developed laminar profile at the channel inlet, and considering ideal gas behavior, this assumption results in the following equation:

$$u = 2\bar{u}^0\left[1-\left(\frac{r}{R}\right)^2\right]\frac{T}{T^0}, \quad (2)$$

which implicitly satisfies the global mass balance.

Model IIc. The axial velocity profile maintains a parabolic shape throughout the reactor:

Table 2. Characteristics of γ-Al_2O_3 Washcoat

Thickness of active catalyst layer	$\delta = 20\ \mu m$
Pore radius	$r_p = 100$ Å
Void fraction	$\epsilon_p = 0.5$

$$u = 2\bar{u}\left[1-\left(\frac{r}{R}\right)^2\right], \tag{3}$$

and the average velocity $\bar{u}$ increases to satisfy the global mass balance

$$2\int_0^R \rho u r\, dr = \rho^0 \bar{u}^0 R^2. \tag{4}$$

Both these models neglect the radial convective transport associated with radial velocity components.

The following additional assumptions have been adopted:

1. Steady-state conditions.
2. Heterogeneous reaction at the catalytic wall with irreversible first-order kinetics in the fuel concentration and zeroth-order in O_2 concentration. These dependencies are in line with indications in the literature of lean fuel–air mixtures (Anderson et al. 1961; Spivey, 1987).
3. The effects of intraporous diffusion have been accounted for by the effectiveness factor approach for an isothermal catalyst. The validity of this hypothesis has been verified by *a posteriori* calculation of T-gradients in the catalyst depth (Smith, 1977). A typical morphology for noble metal catalysts dispersed on a γ-Al_2O_3 washcoat (Table 2) has been assumed, along with an infinite slab geometry.
4. Uniform pressure along the monolith channels in line with the conclusions of Stevens and Ziegler (1977) on the negligible effect of pressure drop on reactant conversion in monoliths reactors. Only in model IId has pressure gradient been included in the momentum balance.
5. Negligible axial diffusion ($Pe_g > 1{,}000$) (Michelsen and Villadsen, 1974).

Moreover heat transfer by solid wall conduction and radiation and the contribution of the homogeneous reaction have been initially neglected. However, their effect on simulation results will be addressed in the following sections.

Governing equations

The assumptions adopted for model IId result in the following set of equations:

Continuity equation

$$\frac{\partial \rho u}{\partial z} + \frac{1}{r}\frac{\partial \rho v r}{\partial r} = 0. \tag{5}$$

Momentum balance in the axial direction

$$\rho\left(u\frac{\partial u}{\partial z} + v\frac{\partial u}{\partial r}\right) = -\frac{dP}{dz} + \frac{1}{r}\frac{\partial}{\partial r}\left(\mu r\frac{\partial u}{\partial r}\right). \tag{6}$$

Enthalpy balance

$$\rho c_p\left(u\frac{\partial T}{\partial z} + v\frac{\partial T}{\partial r}\right) = \frac{1}{r}\frac{\partial}{\partial r}\left(k_{t_g} r\frac{\partial T}{\partial r}\right). \tag{7}$$

Fuel mass balance

$$\rho\left(u\frac{\partial m_f}{\partial z} + v\frac{\partial m_f}{\partial r}\right) = \frac{1}{r}\frac{\partial}{\partial r}\left(D_f \rho r\frac{\partial m_f}{\partial r}\right). \tag{8}$$

Equation of state for ideal gas

$$\rho = \frac{M_g P}{R_g T}. \tag{9}$$

Global mass balance

$$2\pi\int_0^R \rho u r\, dr = \pi R^2 \rho^0 \bar{u}^0, \tag{10}$$

with the relevant boundary conditions:

Inlet conditions ($z = 0$)

$$T = T^0, \quad m_f = m_f^0, \quad v = 0 \quad \forall r, \quad P(0) = P^0 \tag{11}$$

$$u = u^0 \quad \forall r \quad \text{flat inlet velocity profile} \tag{12}$$

$$u = 2\bar{u}^0[1-(r/R)^2] \quad \text{parabolic inlet velocity profile.} \tag{13}$$

Symmetry conditions at the channel axis ($r = 0$)

$$\frac{\partial T}{\partial r} = \frac{\partial m_f}{\partial r} = \frac{\partial u}{\partial r} = 0, \quad v = 0 \tag{14}$$

Wall conditions ($r = R$)

$$\rho D_f \frac{\partial m_f}{\partial r} = -\eta K_c \delta \rho m_f \tag{15}$$

$$k_{t_g}\frac{\partial T}{\partial r} = -\Delta H_r \eta K_c \delta \frac{\rho m_f}{M_f} \tag{16}$$

$$u = 0 \quad \text{no slip condition} \tag{17}$$

$$v = 0 \quad \text{wall impermeability.} \tag{18}$$

For computational reasons the equations have been transformed into the following dimensionless form before numerical solution.

Continuity equation

$$\rho^* \frac{\partial u^*}{\partial z^*} + u^* \frac{\partial \rho^*}{\partial z^*} = -2\left(\frac{\rho^* v^*}{r^*} + \rho^* \frac{\partial v^*}{\partial r^*} + v^* \frac{\partial \rho^*}{\partial r^*}\right). \tag{19}$$

Momentum balance in the axial direction

$$Pe_g\left(\frac{\partial u^*}{\partial z^*}+\frac{\bar{P}}{\rho^* u^*}\frac{dP^*}{dz^*}+2\frac{v^*}{u^*}\frac{\partial u^*}{\partial r^*}\right)=\frac{4\,Pr}{\rho^* u^* r^*}\frac{\partial}{\partial r^*}\left(T^{*0.67}\,r^*\frac{\partial u^*}{\partial r^*}\right). \quad (20)$$

Enthalpy balance

$$Pe_g\left(\frac{\partial T^*}{\partial z^*}+2\frac{v^*}{u^*}\frac{\partial T^*}{\partial r^*}\right)=\frac{4}{\rho^* u^* r^*}\frac{\partial}{\partial r^*}\left(T^{*0.75}\,r^*\frac{\partial T^*}{\partial r^*}\right). \quad (21)$$

Fuel mass balance

$$Pe_g\left(\frac{\partial m_f^*}{\partial z^*}+2\frac{v^*}{u^*}\frac{\partial m_f^*}{\partial r^*}\right)=\frac{4Le}{\rho^* u^* r^*}\frac{\partial}{\partial r^*}\left(T^{*0.75}\,r^*\frac{\partial m_f^*}{\partial r^*}\right). \quad (22)$$

Equation of state for ideal gas

$$\rho^* = P^*/T^*. \quad (23)$$

Global mass balance

$$\int_0^1 \rho^* u^* r^*\, dr^* = \frac{1}{2}. \quad (24)$$

Inlet conditions ($z^* = 0$)

$$T^* = m_f^* = 1 \qquad v^* = 0 \qquad \forall r^*, \qquad P^*(0) = 1 \quad (25)$$

$$u^* = 1 \qquad \forall r^* \qquad \text{flat inlet velocity profile} \quad (26)$$

or

$$u^* = 2[1 - r^{*2}] \qquad \text{parabolic inlet velocity profile} \quad (27)$$

Symmetry conditions at the channel axis ($r^* = 0$)

$$\frac{\partial T^*}{\partial r^*} = \frac{\partial m_f^*}{\partial r^*} = \frac{\partial u^*}{\partial r^*} = 0, \qquad v^* = 0 \quad (28)$$

Wall conditions ($r^* = 1$)

$$\frac{\partial m_f^*}{\partial r^*} = -0.5Da\,T^{*-1.75}\exp\left[\gamma\left(\frac{T^*-1}{T^*}\right)\right]m_f^* \quad (29)$$

$$\frac{\partial T^*}{\partial r^*} = 0.5Da\beta Le\,T^{*-1.75}\exp\left[\gamma\left(\frac{T^*-1}{T^*}\right)\right]m_f^* \quad (30)$$

$$u^* = 0 \qquad \text{no slip condition} \quad (31)$$

$$v^* = 0 \qquad \text{wall impermeability} \quad (32)$$

In models IIb and IIc the continuity equation, Eq. 5, and the momentum balance, Eq. 6, are replaced by Eqs. 2 and 3, respectively, and boundary conditions for u, v, and P^* are no longer necessary. Moreover convective terms in the radial direction are neglected in Eqs. 7 and 8.

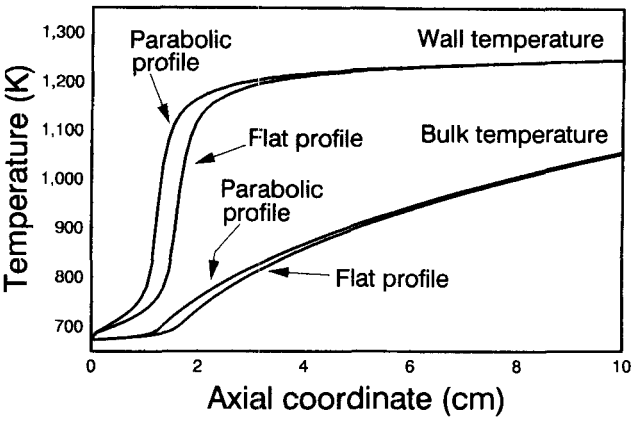

Figure 1. Effect of hydrodynamical development.

$E_{att} = 21{,}550$ cal/mol; $Kc^0 = 125\ s^{-1}$; $T^0 = 673$ K, $Y_f^0 = 0.0218$; $u_{ref} = 7.75$ m/s; $P^0 = 10$ atm; $\epsilon = 0.68$; $d_{eq} = 1.2$ mm.

Model IIa consists of enthalpy and fuel mass balance equations only, with constant gas properties and fully developed laminar velocity profile.

Numerical solution

The set of PDEs of the distributed parameter model was solved numerically using orthogonal collocation techniques, based on symmetric Jacobi polynomials, for the discretization of the dimensionless variable profiles on the radial coordinate of the channel cross section (Finlayson, 1980). The library routine LSODI (Hindmarsh, 1980) was used for integration of the resulting set of initial-value ODEs along the axial coordinate of the monolith reactor.

In order to validate the numerical methods, both the problem of isothermal developing of laminar flow and the Graetz problem in a circular tube with gas property variations with temperature have been solved. Comparison with results in the literature in terms of friction factors, Nusselt numbers, velocity, and temperature profiles (Worsøe-Schmidt and Leppert, 1965; Shah and London, 1978; Bankston and McEligot, 1970) was completely satisfactory. Global momentum and enthalpy balances were satisfied within an error of $\pm 1\%$ all along the channel.

Results and Discussion

Effect of hydrodynamical development

The effect of hydrodynamical development has been investigated by comparing the simulation results obtained with model IId, assuming flat and parabolic velocity profiles at the catalyst inlet, respectively (boundary conditions 12 and 13). Figure 1 gives the axial profiles of wall and bulk temperatures calculated under these assumptions. Typical calculated profiles show that the wall temperature increases along the axial coordinate, with most of the temperature rise confined in a narrow zone, while the gas bulk temperature shows a smoother increment starting from the catalytic light-off due to heat transfer from the ignited catalyst.

A short delay of the light-off is predicted when assuming the velocity profile is flat at the catalyst inlet. Generally, the literature shows that monoliths with worse transfer properties have better light-off performances (Young and Fin-

layson, 1976; Heck et al., 1976; Wilson et al., 1992; Groppi et al., 1993). The reason for this is that in the kinetically controlled regime, which prevails upstream of the catalytic light-off, the gas phase cools the catalytic walls where heat is released due to the occurrence of the exothermic reaction. The enhancement of heat-transfer properties improves the cooling effect, thus delaying and smoothing the light-off process. Thus, the predicted delay is related to the enhancement of the local heat-transfer coefficients due to the hydrodynamical development of laminar profiles, which is well known from the heat-transfer literature (Shah and London, 1978). The gas temperature profiles resulting from the two initial velocity distributions gradually converge downstream of the catalytic light-off, where differences of 10–20 K confined in a limited zone ($\Delta Z \cong 1$–2 cm) have been calculated.

Complete agreement between the predictions of the two models can be obtained by assuming, in the case of parabolic inlet velocity profile, an inlet temperature that is lower by 3–5 K or an activation energy that is lower by 400–600 cal/mole. Since these values are within the experimental uncertainty on these parameters, the assumption of fully developed laminar flow at the catalyst inlet appears to be reasonable.

The results just described show that, despite the short length of the monolith channels (10 cm $\approx$ 0.75 of the length required for complete hydrodynamical development calculated assuming $Re = 2{,}000$ (Shah and London, 1978)), the enhancement of gas–solid heat transfer due to the hydrodynamical development is minor with respect to other controlling phenomena, such as the variation of the gas properties with temperature, which will be discussed in the following section.

Effect of gas property variations

The effect of gas property variations has been investigated by comparing simulation results of models IIa–IId, with IId as the reference model. In view of the results discussed earlier, a parabolic velocity profile at the catalyst inlet has been correctly assumed for model IId, thus uncoupling the effects of gas property variations and of hydrodynamical development.

The calculated axial profiles of the wall and cupmix average temperature are presented in Figures 2a and 2b, respectively. The comparison of the wall temperature profiles predicted by model IIa and IId shows that the former estimates the catalytic light-off to occur earlier than does the latter. This behavior arises from the enhancing effect of temperature on the heat transport properties of the gas phase.

Despite the delay of catalyst ignition, Figure 2b shows that far enough from the light-off model IId predicts a higher gas temperature than model IIa and that the difference increases with the axial length. A temperature difference of about 30–70 K is attained at the monolith outlet for typical catalyst lengths (10–12.5 cm). This result, which is in line with those reported by Bruno et al. (1983), indicates that in the diffusion-limited zone downstream the light-off, the enhancing effect of temperature on the gas transport properties, overcomes the unfavorable effect of the reduced residence time associated with gas speed up due to the temperature dependence of gas density.

The observed discrepancies between gas temperature predictions indicate that the results obtained under the assumption of constant gas properties are not sufficiently accurate, the outlet gas temperature of the catalyst section being one of the most important parameters for determining the extent of the stabilizing effect of the catalyst on the downstream gas-phase combustion.

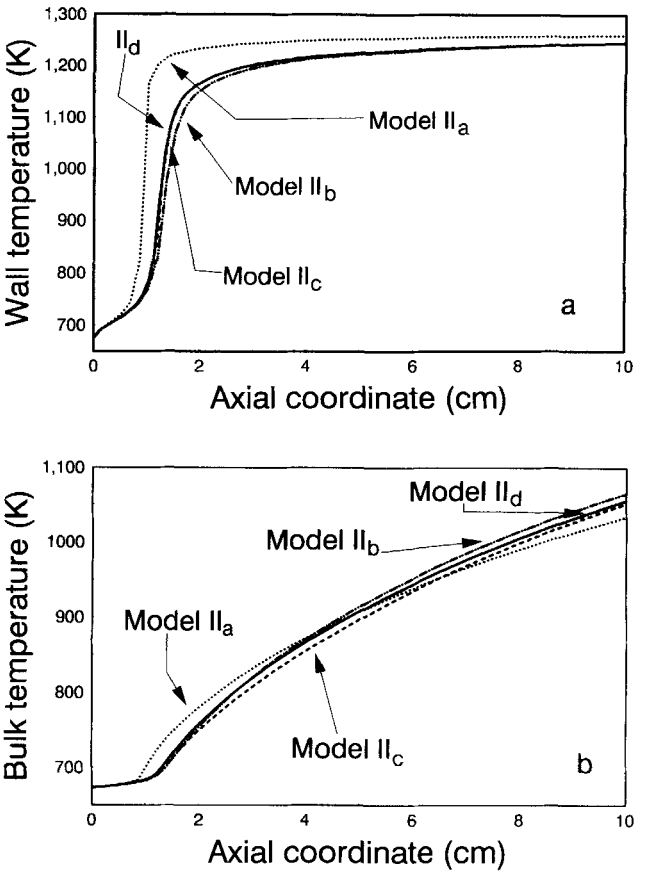

Figure 2. Temperature profiles calculated with different 2-D models.

(a) Wall temperature; (b) gas bulk temperature. $E_{att} = 21{,}550$ cal/mol; $Kc^0 = 125\ s^{-1}$; $T^0 = 673$ K; $Y_f^0 = 0.0218$; $u_{ref} = 7.75$ m/s; $P^0 = 10$ atm; $\epsilon = 0.68$; $d_{eq} = 1.2$ mm.

Figures 2a and 2b show that much more adequate predictions are provided by model IIb and even more accurately by model IIc. In other words, model IIb predicts a slightly delayed light-off and a higher gas temperature ($\Delta T \cong 10$ K) downstream of the catalytic light-off than model IIc, which shows only minor differences with respect to predictions of model IId.

Such deviations are related to the different velocity profiles assumed by models IIb–IId. The radial profiles of the dimensionless specific mass rate (i.e., $\rho^* u^*$) predicted by models IIb–IId at different axial positions are plotted in Figure 3. As imposed by Eq. 2, model IIb assumes a constant specific mass flow at each radial position throughout the reactor. In reality, due to the increment of gas viscosity with temperature, specific mass rates are lowered near the hot catalyst wall, while in the center of the channel the specific mass rate increases to satisfy the global mass balance as predicted by model IId. This eventually results in a decrement of heat- and mass-transfer rates that is neglected by model IIb and is responsible for the delay of the light-off and overesti-

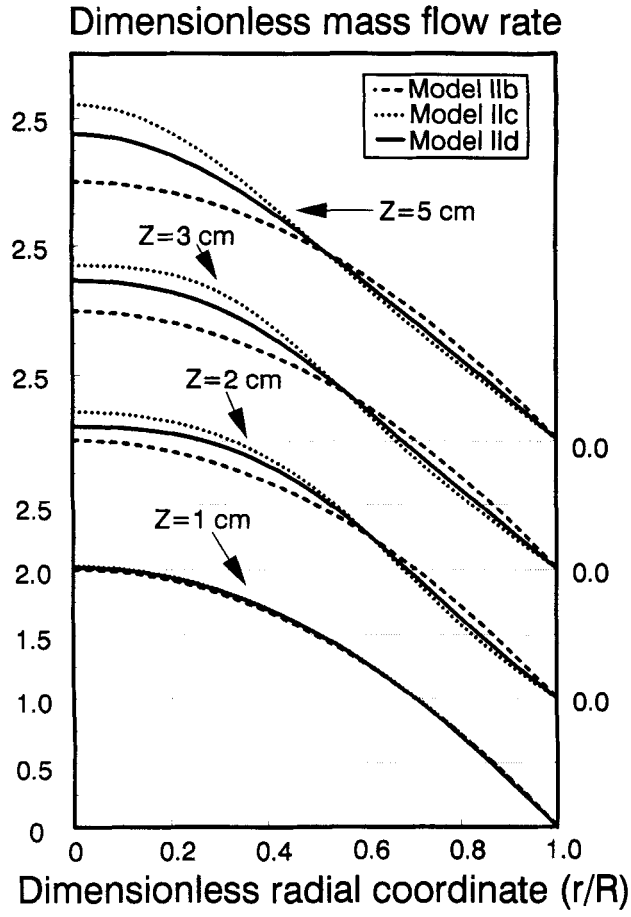

Figure 3. Dimensionless radial profiles of mass-flow rate at different axial locations.

E_{att} = 21,550 cal/mol; $Kc^0 = 125\ s^{-1}$; $T^0 = 673$ K; $Y_f^0 = 0.0218$; $u_{ref} = 7.75$ m/s; $P^0 = 10$ atm; $\epsilon = 0.68$; $d_{eq} = 1.2$ mm.

mation of the gas temperature predicted by this model. Figure 3 also shows that the specific mass rate profiles predicted by model IIc are only a little more narrow than those predicted by model IId. Thus, very accurate temperature predictions are obtained with model IIc.

The small differences between the results of models IIc and IId can be explained by considering the profiles of calculated radial velocity at the different axial positions plotted in Figure 4. Upstream of the catalytic light-off (curves at $z = 0.5$ cm and $z = 1$ cm), the radial velocities are close to zero, while immediately after catalyst ignition ($z = 1.65$ cm), they become appreciable and centripetal due to the steep increase of wall heat flux and temperature, which result in a novel thermal and hydrodynamical development. The magnitude of the radial velocity components in the light-off region are close to those arising from cold hydrodynamical development in the same axial position. A limited enhancement of transport properties is associated with these centripetal convection terms that lead to a slightly faster heating of the gas phase: this can be observed in Figure 2b immediately after the light-off. Further downstream from the light-off ($z > 4$ cm), the radial velocities rapidly diminish until inversion occurs and velocities become centrifugal. Subsequently, the heat-transfer rate is slightly decreased, and consequently the gas tempera-

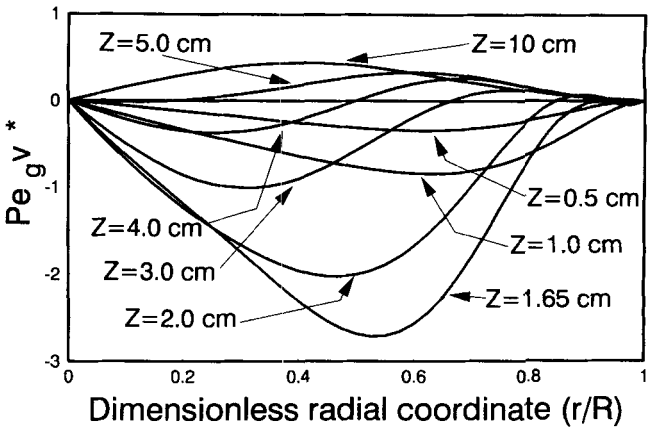

Figure 4. Radial profiles of dimensionless radial velocity at different axial locations.

E_{att} = 21,550 cal/mol; $Kc^0 = 125\ s^{-1}$; $T^0 = 673$ K; $Y_f^0 = 0.0218$; $u_{ref} = 7.75$ m/s; $P^0 = 10$ atm; $\epsilon = 0.68$; $d_{eq} = 1.2$ mm.

ture rise predicted by model IId is a little slower than that predicted by model IIc. However, the largest discrepancies between model IIc and IId predictions are less than 10 K. Accordingly, model IIc-type approximation can be adopted: it provides reasonably accurate results with a saving of computational time exceeding one order of magnitude.

Effect of wall conduction and radiation

In view of the steep axial T-gradients that prevail in the combustor, backward heat transmission by wall conduction and radiation may be expected to affect model predictions. To quantitatively assess this effect, the terms related to wall conduction have been introduced in the governing equations of model IIc. Accordingly Eq. 16 has been transformed into equation

$$\frac{(1-\epsilon)}{\epsilon}\frac{d_{eq}}{4}k_t\frac{\partial^2 T}{\partial z^2} - k_{t_g}\frac{\partial T}{\partial r} - \Delta H_r \eta K_c \delta \frac{\rho m_f}{M_f} = 0 \qquad \text{at} \quad r = R, \quad (33)$$

which is derived from the enthalpy balance of the solid phase under the assumption of constant temperature of the solid in the radial direction and the imposition of the equivalence of solid and gas temperatures at the phase interface. Equation 33 has been rewritten in dimensionless form before solution

$$\frac{1}{8}\frac{(1-\epsilon)}{\epsilon}\frac{Pe_g}{Pe_s}T^{*-0.75}\frac{\partial^2 T^*}{\partial z^{*2}} - \frac{\partial T^*}{\partial r^*} + \frac{1}{2}DaLe\beta T^{*-1.75}\exp\left(\gamma\left(\frac{T^*-1}{T^*}\right)\right)m_f^* = 0 \qquad \text{at} \quad r^* = 1. \quad (34)$$

Moreover the following relevant boundary conditions have been considered:

$$\frac{\partial T}{\partial z} = 0 \quad \text{at} \quad z = 0 \quad \text{and} \quad z = L \qquad (35)$$

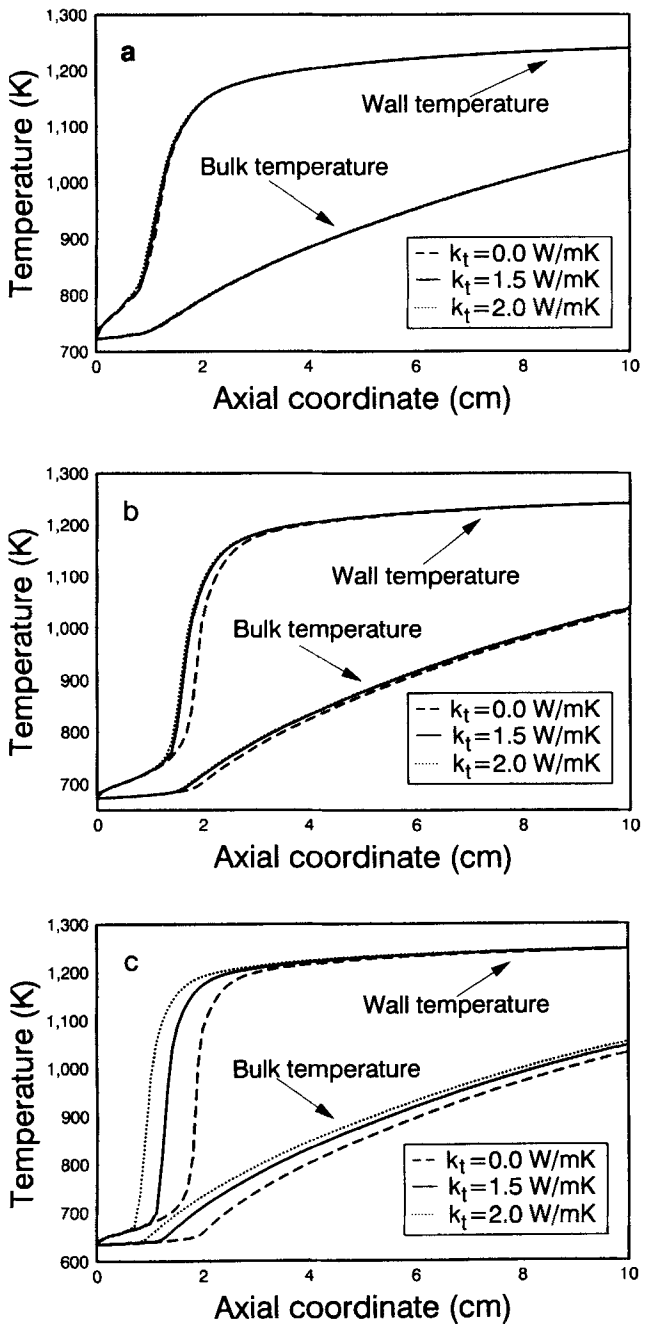

Figure 5. Effect of solid thermal conductivity in ceramic monoliths.

(a) $T^0 = 723$ K; $Y_f^0 = 0.0200$; $\Delta T_{ad} = 550$ K; $K_c^0 = 175$ s^{-1}; (b) $T^0 = 673$ K; $Y_f^0 = 0.0218$; $\Delta T_{ad} = 600$ K; $K_c^0 = 105$ s^{-1}; (c) $T^0 = 623$ K; $Y_f^0 = 0.0230$; $\Delta T_{ad} = 650$ K; $K_c^0 = 85$ s^{-1}. $E_{att} = 21{,}550$ cal/mol; $u_{ref} = 7.75$ m/s; $P^0 = 10$ atm; $\epsilon = 0.68$; $d_{eq} = 1.2$ mm.

and in dimensionless form

$$\frac{\partial T^*}{\partial z^*} = 0 \quad \text{at} \quad z^* = 0 \quad \text{and} \quad z^* = L/d_{eq}. \tag{36}$$

It is worth noticing that according to Lee and Aris (1977) the contribution of radiation also can be simulated by enhancing the value of solid conduction to account for the additional backward heat transfer.

The resulting boundary value problem along the axial coordinate strongly enhances the computational cost of the solution. Orthogonal collocations on finite elements (Finlayson, 1980) have been adopted for axial integration using third-order polynomials over each finite element for profile simulation. Convergence has been achieved with 10–12 internal grid points. Simulations have been performed for wall conductivities from 1.5 to 25 W/mK, that is, the typical values for ceramic and metallic monoliths, respectively.

Figures 5a–5c present the axial profiles of T-wall and T-bulk calculated for three different gas inlet temperatures and for three values of solid conduction k_t:W/m·K$k_t = 0$ has been included as a reference; $k_t = 1.5$ W/m·K corresponds to the thermal conductivity of cordierite; $k_t = 2$ W/mK has been calculated by enhancing the value of cordierite according to the formula proposed by Lee and Aris (1977) in order to account for the contribution of radiative heat transfer:

$$k_r = \frac{16}{3}\sigma r T_s^3 \Psi(\chi) \tag{37}$$

with

$$\Psi(\chi) = 1 + \frac{\chi^3}{4} - \frac{\chi^2\sqrt{\chi^2+1}}{4} + \frac{\sqrt{\chi^2+1}}{8} - \frac{9}{8\chi}\ln\left(\chi + \sqrt{\chi^2+1}\right). \tag{38}$$

In spite of the high temperature of the catalytic wall ($\approx 1{,}273$ K), the calculated enhancement is noticeably small due to the high aspect ratio of the monolith channels ($\chi \approx 100$).

The results plotted in Figures 5a–5c show that the effect of wall conduction is also negligible for ceramic monoliths when including the contribution of radiation. A slight upstream shift of the catalytic light-off is predicted only for the most severe case corresponding to the lowest inlet temperature (623 K). On decreasing the inlet temperature both dimensionless activation energy and adiabatic temperature rise increase so that T-gradients in the light-off region become sharper. However, in this case the differences between predicted gas temperatures are also limited and mostly confined near the light-off region. Moreover, such an inlet temperature appears rather optimistic with respect to reasonable values of catalyst activity in CH_4 oxidation.

In spite of the steep T-gradients of the profile, such a lack of influence of wall conduction is at variance with the indications in the literature of the simulation of similar monolith reactors used as catalytic mufflers. This discrepancy arises from the high mass-flow rates prevailing in hybrid combustors. For example, the values of mass-flow rates, herein assumed in the simulations, correspond to the lower limit of the operational range of the combustor and are one order of magnitude higher than those typical of catalytic mufflers. For such mass-flow rates, heat transfer along the axis due to wall conduction is negligible compared to the convective contribution. It is worth noting that this result can be reasonably extended to the highest flow rates in the operational range of

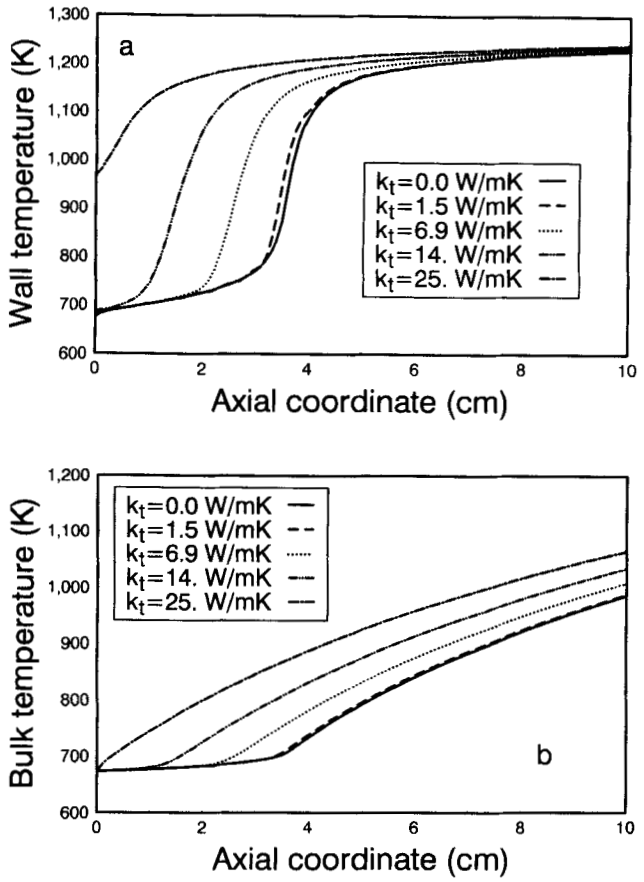

Figure 6. Effect of axial heat conduction in monoliths with different solid thermal conductivities.

(a) Wall temperature; (b) gas bulk temperature. $E_{att} = 21{,}550$ cal/mol; $P^0 = 10$ atm; $T^0 = 673$ K; $\Delta T_{ad} = 600$ K; $Y_f^0 = 0.0218$; $K_c^0 = 80\ s^{-1}$; $u_{ref} = 7.75$ m/s; $\epsilon = 0.68$; $d_{eq} = 1.2$ mm.

the hybrid combustor corresponding to the transitional and turbulent hydrodynamical regimes.

As might be expected, the picture gradually changes as the solid conductivity increases. Figures 6a and 6b show the axial profiles of T-bulk and T-wall calculated for k_t up to 25 W/mK, that is, the value reported in the literature for metallic monoliths (Kolaczowski et al., 1988). The calculated light-off position shifts gradually upstream on increasing the solid conductivity due to the growing importance of backward heat transmission. The improvement of the light-off performances results in an increment of the gas bulk temperature due to the enhanced heat released by the catalytic walls. The difference between calculated gas exit temperatures points out that wall conduction cannot be neglected when simulating metallic monoliths. Moreover the results in Figure 6a and 6b indicate that the use of metallic monoliths would result in better combustor performances in terms of gas heating in the catalyst section and of the related stabilizing effect on downstream homogeneous combustion. At present, however, metallic monoliths cannot withstand the severe thermal shocks occurring in gas turbine combustors.

When simulating combustor monoliths, the problem of multiple steady-state solutions (MSSS) should also be addressed. In principle, steady-state multiplicity can occur in hybrid combustors due to the strong nonlinear interaction between thermal effects and chemical kinetics. Multiple steady states were experimentally observed by Prasad and coworkers (Prasad et al., 1981) for propane combustion in monolith catalysts. With reference to this problem models with and without wall conduction terms are intrinsically different. The former models may predict MSSS associated with backward heat transfer, while the mathematical structure of the equations of distributed parameter models without wall conduction do not allow MSSS (Young and Finlayson, 1976). To clarify the relevance of this problem, the occurrence of MSSS has been investigated by means of the model including wall conduction. Simulation results show that no MSSSs are predicted for typical operating and kinetic parameters of the catalytic channels. Thus, neglect of wall conduction does not result in any loss of information (other possible steady-state solutions).

The capability of the model including wall conduction and the related method of numerical solution in predicting multiple steady states has been checked by exploring parametric regions outside the typical domain for hybrid combustor operation. As shown in Figures 7a–7c, multiple solutions have been predicted for an activation energy of 25 kcal/mol (a higher value than those expected for actual combustion catalysts). Three steady-state solutions typically have been found for intermediate values of k_t (Figures 7a and 7b). Steady-state multiplicity disappears both on decreasing k_t, the three solutions collapsing onto the lowest one, and on increasing k_t, the three solutions collapsing onto the highest one (Figure 7c).

The results described earlier suggest that the contributions of wall conduction and radiation can be reasonably neglected in the simulation of ceramic monoliths for hybrid combustor applications. This approximation allows for a strong saving of the computational time for numerical solution (about two orders of magnitude). It has to be stressed once more, however, that the validity of this conclusion is strictly limited to the operating conditions of the hybrid combustor and to the use of insulating material for monolith construction. In fact, important effects of backward heat transfer are predicted on decreasing the mass-flow rate, on increasing the maximum wall temperature, and on increasing the thermal conductivity of the solid.

It is worth noticing that neglecting wall conduction with no loss of accuracy may be of relevance when considering the problem of the adequacy of simpler one-dimensional models. Results in the literature (Young and Finlayson, 1976) demonstrate that lumped models accounting for wall conduction always arrive at misleading results. The problem of the adequacy of lumped parameter models in the simulation of the monolithic catalyst in hybrid combustors is the subject of a companion article (Groppi et al., 1995).

Effect of the homogeneous reaction

It has been experimentally demonstrated that homogeneous reactions play a fundamental role in monolith catalysts of CST combustors. On the other hand, gas-phase combustion is believed to be less important in the catalytic section of the hybrid combustors. To verify this point the effect of the homogeneous reaction on methane conversion and gas bulk temperature within the catalytic bed has been investigated.

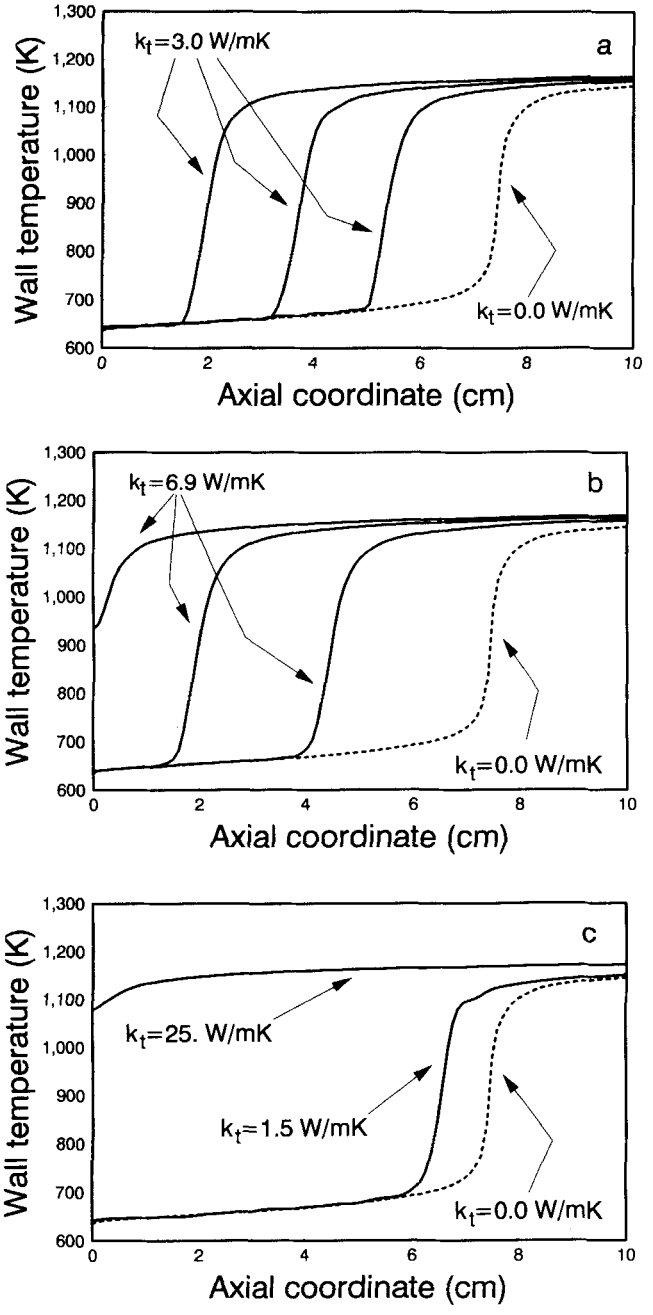

Figure 7. Multiple steady-state solutions.

(a) $k_t = 3.0$ W/m·K. (b)$k_t = 6.9$ W/m·K. (c) $k_t = 25$ W/m·K and $k_t = 1.5$ W/m·K. $E_{att} = 25{,}000$ cal/mol; $P^0 = 10$ atm; $T^0 = 638$ K; $Y_f^0 = 0.023$; $K_c^0 = 45$ s^{-1}; $u_{ref} = 7.75$ m/s; $\epsilon = 0.68$; $d_{eq} = 1.2$ mm.

Two-dimensional models appear to be particularly well suited for this purpose because they account for the radial distribution of temperature, thus being able to predict the ignition of the homogeneous reaction in the boundary layer of the catalytic walls. The relevant terms for the homogeneous reaction have therefore been introduced in the mass and heat balance equations of model IIc. The simplified two-step molecular kinetics proposed by Dryer and Glassman (1972) for methane lean combustion has been implemented.

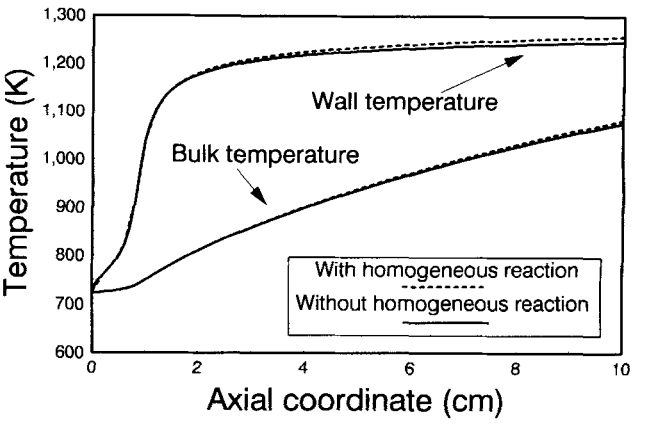

Figure 8. Effect of gas-phase reaction in the catalytic section of a hybrid combustor.

$E_{att} = 21{,}550$ cal/mol; $K_c^0 = 200$ s^{-1}; $T^0 = 723$ K; $Y_f^0 = 0.0200$; $u_{ref} = 7.75$ m/s; $P^0 = 10$ atm; $\epsilon = 0.68$; $d_{eq} = 1.2$ mm.

Figure 8 presents the axial profiles of bulk and wall temperature calculated with and without the homogeneous reaction contribution. No appreciable differences are observed between the profiles, thus confirming that the homogeneous combustion likely plays a negligible role in the catalytic section of natural-gas-fueled hybrid combustors due to the combined effects of limited temperatures (T-bulk < 1,073 K; T-wall ≤ 1,273 K) and very short residence times (a few milliseconds). Thus, these results can be reasonably extended to the entire operational range of gas-flow rates of the hybrid combustor.

Notice that the effect of the homogeneous reaction would be no longer negligible in the case of fuels that can be more easily oxidized than methane such as a CO/H_2 mixture from coal gasification.

However, for natural gas fuel a role of the homogeneous combustion also cannot be definitely excluded in view of possible interactions between the kinetics of homogeneous and heterogeneous reactions (such as catalytic walls acting as radical sources). Such effects have not been considered in the simplified kinetic treatment adopted here.

Conclusions

Development and solution of rigorous and simplified 2-D models of the single channel in the monolith combustors has allowed a quantitative assessment of the importance of various phenomena occurring in the catalytic section of a hybrid combustor for gas turbines. Thus, the simplest distributed parameter model that can provide adequate predictions has been identified.

In summary, simulation results point out the following major aspects:

1. To obtain adequate predictions variations of gas properties have to be taken into account in view of the strong T-gradients prevailing in the monolith channels. On the other hand, the rigorous solution of momentum balance and continuity equations used to determine the actual gas velocity profiles can be avoided by assuming an invariant parabolic shape of the radial profile of axial velocity. In fact, the effects of the hydrodynamical development and of the deformation of the

velocity profile associated with the variations of gas viscosity are negligible.

2. Limited to the specific operating conditions of the hybrid combustors, the backward heat transfer by wall conduction can be neglected in the simulation of ceramic monoliths. This allows for a significant saving of computational time.

The effect of wall heat conduction is of growing importance on increasing the maximum wall temperature (in CST combustors), decreasing the mass-flow rate (in catalytic mufflers), and increasing the solid conduction (in metallic monoliths). No multiple steady-state solutions arise from backward heat transfer for typical operating parameters of the hybrid combustor.

3. The contribution of homogeneous combustion can be safely neglected in the catalytic section of a hybrid combustor fueled by natural gas.

Although the results herein reported refer to the monoliths with circular channels, the conclusion on model sensitivity to various chemicophysical phenomena can be reasonably generalized to other channel shapes, such as square and triangle.

Acknowledgments

This study has been supported by the CNR-ENEL Project—Interactions of energy systems with human health and environment—Rome, Italy.

Notation

A = cross-sectional area
C = concentration, mol/cm^3
c_p = heat capacity of gas at constant pressure, per unit mass, kJ/(kg·K)
d_{eq} = 4 (cross-sectional area of tube)/(wetted perimeter), m
D = molecular diffusion coefficient, m^2/s
$Da = (\eta K_c^0 \delta d_{eq})/D^0$ = Damköhler number
E_{att} = activation energy, kJ/kmol
$Gr = (8 g \rho_g^2 R^3)/\mu_g$ = modified Grashof number
ΔH_r = heat of reaction, kJ/kmol
K_c = intrinsic rate constant, s^{-1}
k_r = equivalent conductivity for radiation, W/(m·K)
L = channel length, m
$Le = D^0/\alpha^0$ = Lewis number
m = mass fraction
M = average molecular weight, kg/kmol
P = absolute pressure, atm
$P^* = P/P^0$ = dimensional pressure
$\overline{P} = P^0/(\rho^0 \bar{u}^{0^2})$
$Pe_g = (\bar{u}^0 d_{eq})/\alpha_g^0$ = gas Peclet number
$Pe_s = (\bar{u}^0 d_{eq})/\alpha_s^0$ = solid Peclet number
$Pr = \mu c_p/k_t$ = Prandtl number
r = radial coordinate, m
$r^* = r/R$ = dimensionless radial coordinate
r_p = pore radius, Å
R = channel radius, m
$Re = (\rho \bar{u} d_{eq})/\mu$ = Reynolds number
R_g = gas constant, kJ/(kmol·K)
T = temperature, K
u = axial velocity, m/s
$\bar{u}$ = average cupmix velocity, m/s
$u^* = u/\bar{u}^0$ = dimensionless axial velocity
u_{ref} = gas velocity at the cross section immediately upstream the channel inlet, m/s
v = radial velocity, m/s
$v^* = v/\bar{u}^0$ = dimensionless radial velocity
Y = molar fraction
z = axial coordinate, m
$z^* = z/d_{eq}$ = dimensionless axial coordinate

Greek letters

$\alpha = k_t/\rho c_p$ = thermal diffusivity, m^2/s
$\beta = (m_f \Delta H_r)/(M_f c_p T^0)$ = dimensionless adiabatic temperature
$\gamma = E_{att}/R_g T^0$ = dimensionless activation energy
δ = thickness of active catalyst layer
ϵ = open frontal area
ϵ_p = catalyst void fraction
$\eta = \tanh\phi/\phi$ = effectiveness factor
μ = viscosity, kg/m·s
ρ = gas density, kg/m^3
$\rho^* = \rho/\rho^0$ = dimensionless gas density
σ = Stefan–Boltzmann constant, $1{,}355 \times 10^{-12}$ cal/(s·cm^2·K^4)
$\phi = \delta\sqrt{K_c/D_{eff}}$ = Thiele modulus
$\chi = L/d$ = channel aspect ratio

Subscripts and superscripts

0 = inlet conditions
$*$ = dimensionless variable
b = bulk conditions
w = wall conditions
f = fuel
g = gas
s = solid
S = catalyst surface

Literature Cited

Anderson, R. B., K. C. Stein, J. J. Feenan, and L. J. E. Hofer, "Catalytic Oxidation of Methane," *Ind. Eng. Chem.*, **53**, 809 (1961).

Bankston, C. A., and D. M. McEligot, "Turbulent and Laminar Heat Transfer to Gases with Varying Properties in the Entry Region," *Int. J. Heat Mass Transf.*, **13**, 319 (1970).

Bruno, C., P. M. Walsh, D. A. Santavicca, N. Sinha, Y. Yaw, and F. V. Bracco, "Catalytic Combustion of Propane/Air Mixture on Platinum," *Comb. Sci. Technol.*, **31**, 43 (1983).

Dryer, F. L., and I. Glassman, "High-Temperature Oxidation of CO and CH_4," *Proc. 14th Symp. (Int.) on Combustion*, The Combustion Institute, p. 987 (1972).

Finlayson, B., *Nonlinear Analysis in Chemical Engineering*, McGraw Hill, New York (1980).

Furuya, T., T. Hayata, S. Yamanaka, J. Koezuka, T. Yoshine, and A. Ohkoshi, "Hybrid Catalytic Combustion for Stationary Gas Turbine-Concepts and Small Scale Test Results," ASME Paper No. 87-GT-99, 1 (1987).

Groppi, G., E. Tronconi, and P. Forzatti, "Modelling of Catalytic Combustors for Gas Turbine Applications," *Catalysis Today*, **17**, 237 (1993).

Groppi, G., A. Belloli, E. Tronconi, and P. Forzatti, "On the Adequacy of One-Dimensional Models of Monolith Catalysts in Hybrid Combustors for Gas Turbines," *Chem. Eng. Sci.*, **50**, 2705 (1995).

Hayes, R. E., S. T. Kolaczkowski, and W. J. Thomas, "Finite-Element Model for a Catalytic Monolith Reactor," *Comp. Chem. Eng.*, **16**, 645 (1992).

Heck, R. H., J. Wei, and J. R. Katzer, "Mathematical Modeling of Monolithic Catalysts," *AIChE J.*, **22**, 477 (1976).

Hindmarsh, A. C., "LSODE and LSODI, Two New Initial Value Ordinary Differential Equation Solvers," *ACM-Signum Newsletter*, **15**, 10 (1980).

Kolaczowski, S. T., P. Crumpton, and A. Spence, "Modelling of Heat Transfer in Non-Adiabatic Monolithic Reactors," *Chem. Eng. Sci.*, **43**, 227 (1988).

Lee, S. T., and R. Aris, "On the Effects of Radiative Heat Transfer in Monoliths," *Chem. Eng. Sci.*, **32**, 827 (1977).

Michelsen, M. L., and J. Villadsen, "The Graetz Problem with Axial Heat Conduction," *Int. J. Heat Mass Transf.*, **17**, 1391 (1974).

Ozawa, Y., J. Hirano, M. Sato, M. Saiga, S. Watanabe, and M. Okahata, "Preliminary Test Results of Catalytic Combustor for Gas Turbine," *Proc. JECAT'91*, Tokyo, **P30**, 302 (1991).

Pfefferle, L. D., and W. C. Pfefferle, "Catalysis in Combustion," *Catal. Rev. Sci. Eng.*, **29**, 219 (1987).
Prasad, R., L. A. Kennedy, and E. Ruckenstein, "Catalytic Combustion," *Catal. Rev. Sci. Eng.*, **26**, 1 (1984).
Prasad, R., H. L. Tsai, L. A. Kennedy, and E. Ruckenstein, "Occurrence of Multiple Steady States in the Catalytic Combustion of Propane," *Comb. Sci. Technol.*, **26**, 51 (1981).
Schlichting, H., *Boundary Layer Theory*, McGraw-Hill, New York (1955).
Shah, R. K., and A. L. London, *Laminar Flow Forced Convection*, Academic Press, New York (1978).
Smith, T. G., "An Examination of the Isothermal Pellet Assumption Relative to the Design of Nonadiabatic Fixed Bed Catalytic Reactors," *Chem. Eng. Sci.*, **32**, 1023 (1977).
Spivey, J. J., "Complete Catalytic Oxidation of Volatile Organics," *Ind. Chem. Res.*, **26**, 2165 (1987).
Stevens, J. G., and E. N. Ziegler, "Effect of Momentum Transport on Conversion in Adiabatic Catalytic Tubular Reactors," *Chem. Eng. Sci.*, **32**, 385 (1977).
Trimm, D. L., "Catalytic Combustion," *Appl. Catalysis*, **7**, 249 (1983).
Young, L. C., and B. A. Finlayson, "Mathematical Models of the Monolith Catalytic Converter. Part II: Application to Automobile Exhaust," *AIChE. J.*, **22**, 331 (1976).
Wilson, G. C., M. F. Bardon, and J. J. Witton, "Experimental and Computational Investigation of Flow in Catalytic Monolith Channels," ASME Paper 92-GT-118, 1 (1992).
Worsøe-Schmidt, P. M., and G. Leppert, "Heat Transfer and Friction for Laminar Flow of Gas in a Circular Tube at High Heating Rate," *Int. J. Heat Mass Transf.*, **8**, 1281 (1965).

Manuscript received July 19, 1994, and revision received Nov. 16, 1994.